GGD 37: The Fastest Protostellar Outflow?

J. D. Green[1], D. A. Neufeld[2], D. M. Watson[3], E. Bergin[4],S. Maret[4],G. Melnick[5],P. Sonnentrucker[6], V. Tolls[5], B. A. Sargent[6], W. J. Forrest[3], K.H. Kim[3], & S. N. Raines[7]

1. Department of Astronomy, University of Texas at Austin; 2. Department of Astronomy, The Johns Hopkins University; 3. Department of Physics and Astronomy, University of Rochester, Rochester, NY 14627; 4. Department of Astronomy, University of Michigan; 5. Harvard-Smithsonian Center for Astrophysics, 60 Garden St., Cambridge, MA 02138; 6. Space Telescope Science Institute, Baltimore, MD; 7. Department of Astronomy, University of Florida, Gainesville, FL

ABSTRACT

We present the first Spitzer-IRS spectral maps of a Herbig Haro flow detected in lines of [Ne III], [O IV], [Ar III], and [Ne V] in GGD 37 (Cep A West). The extended detection of [O IV] (55 eV required to create) and some extended emission in [Ne V] (97 eV) indicates a shock temperature in excess of 100,000 K, in agreement with X-ray observations, and a shock speed in excess of 200 km s^{-1}. The presence of an extended photoionization or collisional ionization region indicates that GGD 37 is a highly unusual protostellar outflow.

Subject headings:

1. Introduction

1.1. The Consequences and Causes of Protostellar Accretion

Spinning protostellar cores of protostars of all masses eject material in the form of detectable bipolar outflows when their accretion rates are sufficiently high, ie. $\gtrsim 10^{-7}$ $M_\odot\,yr^{-1}$. Very massive stars may trigger additional star formation through these powerful flows. Even the much more numerous outflows from low mass stars may impact their local environment with high velocity flows and stir up turbulence, but it is unclear how far their ejecta can travel before dissipating. Intermediate mass stars are an interesting middle scenario: are they numerous enough and powerful enough to trigger further star formation, or suppress it?

Shocks were categorized by their physics in Draine (1980): J-type shocks in which the magnetic field from the shocked ions is either frozen into the shock, or is non-existent; J-type shocks with magnetic precursors (or radiative precursors), in which the neutral fluid undergoes a discontinuous "jump" in density and temperature; and C-type shocks in which the fluid changes continuously over the shock boundary. The density and temperature conditions in these shocks vary and can be constrained through observations of fine structure line emission with differing appearance potential and critical density.

At 700 pc distant, the Cepheus A cloud complex contains some of the best observed Herbig Haro objects. Cep A consists of at least two broadly extended CO outflows, Cep A East and Cep A West (Hughes & Wouterloot 1982); the latter sometimes referred to as GGD 37 or HH 168 (Reipurth & Raga 1999). Both flows have been mapped by Spitzer-IRS (Sonnentrucker et al. 2006; Neufeld et al. 2006a). The extinction toward GGD 37 is generally thought to be small (Froebrich et al. 2002) but Wright et al. (1996) apply an A_V of 16 to their data.

The Cep A region has been mapped in both hard and soft X-rays with XMM-Newton (Pravdo & Tsuboi 2005; Pravdo et al. 2009) and Chandra (Schneider et al. 2009). Both HW2 and HW3c are detected in hard X-rays, while HH 168 (including the W1-W2-W3 region) is detected in soft X-rays. Pravdo & Tsuboi (2005) note several distinct soft X-ray sources within HH 168 flow, one near the W2 region, and one at the far end of the flow. They conclude for GGD 37 that $L_X = 3 \times 10^{30}$ erg s^{-1}, and infer a shock velocity of 620 km s^{-1}, and a temperature of 4×10^6 K from comparisons to L1551-IRS 5 / HH 154 (Favata et al. 2002; Bally et al. 2003). They observe that the flow is extreme in temperature, although not in luminosity. The X-ray emissions are offset from both the optical and radio emissions, and they conclude this is due to the complex morphology of the region and multiple driving sources, as well as anisotropy in the medium. In this paper we conclude that the offset and extended nature of the soft X-ray emission is directly tied to the cloud shock.

2. Observations and data reduction

We utilized Spitzer-IRS to observe GGD 37 as part of our guaranteed and general observing time (program 2, PI: J.R. Houck; program 30167, PI: D. A. Neufeld); for the full dataset, see Green et al. (2010a, in prep.). We observed this region in a Spitzer-IRS map grid consisting of two adjacent rectangles, on two separate occasions; first in SH and LH in 2004, and again in SL and in deeper exposures in LH in 2007. These maps cover approximately the same regions of the sky, although Cep A East was observed concurrently with the first set of observations of GGD 37. The resolution of individual pixels of the IRS is given in the

Spitzer Observers' Manual [1] as ranging from $\sim$ 2 - 5 arcsec squares, depending upon the module in question; therefore the maps contain differing spatial resolution, although they have all been regridded and oversampled for display purposes.

For full details of the data reduction process, see Green et al. (2010a); here we briefly summarize the procedure. The basic calibrated data (BCD) were processed at the Spitzer Science Center (SSC) using version S12.0, S15.3, or S17.2 of the processing pipeline, and then reduced using SMART, modified by additional routines that we have developed to deal with map grids (as opposed to single observation staring mode). We process the data beyond the traditional SMART reduction by removing bad pixels in all modules, using a "grand" rogue mask created from a superposition of the bad pixel masks of each separate observing campaign. Rogues that occur once at the 4σ level are considered to be permanently bad pixels and thus the grand rogue mask contains 25% more rogue pixels than a single campaign rogue mask. Bad pixels are fixed using a nearest neighbor routine (imclean.pro and imnan.pro).

Next we extracted individual spectra using a modified version of SMART, not simply from each slit position, but from each individual resolution element of each slit position. In the case of SH and LH, we produce five (semi-)independent spectra, spatially separated by the resolution of a single pixel in the array; in SL we use 32 independent positions to generate spectra. The spectra are then re-gridded onto a regular grid in RA and declination. Pixels with (nearly) identical positions are averaged together. We apply the slit loss correction function (SLCF; J. D. Smith, private communication) to correct for flux-calibration created for point-sources, used by the Spitzer Science Center. The result is a downward correction to the flux to $\sim$ 60-90% of the original value.

2.1. Extended Detection of Lines with Appearance Potential > 13.6 eV

We report the first detection of [Ar III], [Ne III], [O IV] or [Ne V] in a Herbig-Haro flow. Many of lines of lower excitation species, including [Ne II], [Si II], and [S I] were detected in GGD37 in Wright et al. (1996) with ISO-SWS; however strong detections such as [Ne III] are not reported; this may be due to the large beam size of ISO and the small spatial extent of the [Ne III] emission. Despite its relatively weak flux, the [O IV] detection appears to be clean and spatially differentiated from the partially blended [Fe II] emission, although it tracks the [Fe II] knots broadly. Guiles et al. (2007) observed emission from apparent spectral lines several resolution elements on both sides of extremely bright lines in their sources, but they were ascribed to data artifacts due to the symmetric nature of the "lines"

[1] http://ssc.spitzer.caltech.edu/documents/som/

around the central peak. In this case the [Fe II] line brightness is not extreme and there is no corresponding bump on the long-wavelength side of the [Fe II] 26 μm line. The [Ar III] map is co-spatial with the other lines, with the exception that it appears to contribute to the westernmost clump in the map, unlike the other species of higher appearance potential. Additionally there is a possible detection of [Ar III] (8.99 μm) but it is suspect due to lack of coherence in its mapped spatial structure (Green et al. 2010a, in prep.).

The [Ne V] emission is confined to the area around W2 and a point at the northwest end of the flow (Figure 2), roughly coinciding with the edge of the lower excitation line emission from [Fe II]. Raines (2000, his figure 3.15) noted that the peak of the [Fe II] (1.644 μm) emission was shifted to the east by $\sim$ 3 arcseconds from the peak of the H_2 (2.122 μm) emission; we note a similar result in our maps–although the spatial resolution is considerably lower than in Raines' images – and we can clearly see that the peak emission from all of the ionized species is located east of the peak of the H_2 S(1) - S(7) emission. Additionally, the higher ionization species appear to be themselves shifted eastward by a further $\sim$ 5" compared to the lower ionization species, suggesting that we are resolving the postshock region (Figure 3)

3. Discussion

Originally detected as a radio emitter by Hughes & Wouterloot (1982) and resolved into three separate components (W1, W2, and W3) by Hughes (1989) using VLA data, W2 is a prime candidate for an intermediate mass protostellar object driving an exceptionally powerful outflow (Garay et al. 1996). The edge of the GGD 37 flow is approximately located at Source S as defined in Hartigan & Lada (1985), and the W2 and S locations coincide with a line of soft X-ray emission (Pravdo & Tsuboi 2005), as well as velocity-resolved [O III] (5007 nm) emission in the case of Source S (Hartigan et al. 1986). Pravdo & Tsuboi (2005) identify W2 and S as separate exciting sources for soft X-rays, although they observe significant emission from the line connecting the two as well, and the [O III] emission has linewidths of $\sim$ 420 km s^{-1}. It is therefore not very surprising that that such highly ionized species as O+++ and Ne++++ are present; these ions trace the hottest gas and provide constraints on the shock energetics.

Our data support the identification of GGD 37 as a protostellar outflow originating at W2. The continuum spectral index α is defined as $d\ log(\lambda\ F_\lambda)/\ d\ log(\lambda)$. Calculated at the position of the W1-2-3 aperture (Table 1) $\alpha \sim 1$ when measured from 5.5 to 10 μm and $\sim$ 3 when measured from 10 to 35 μm, both results in the range typical of Class 0/I YSOs. Our data reveal spectral lines with extremely high excitation potentials, ranging up to 97

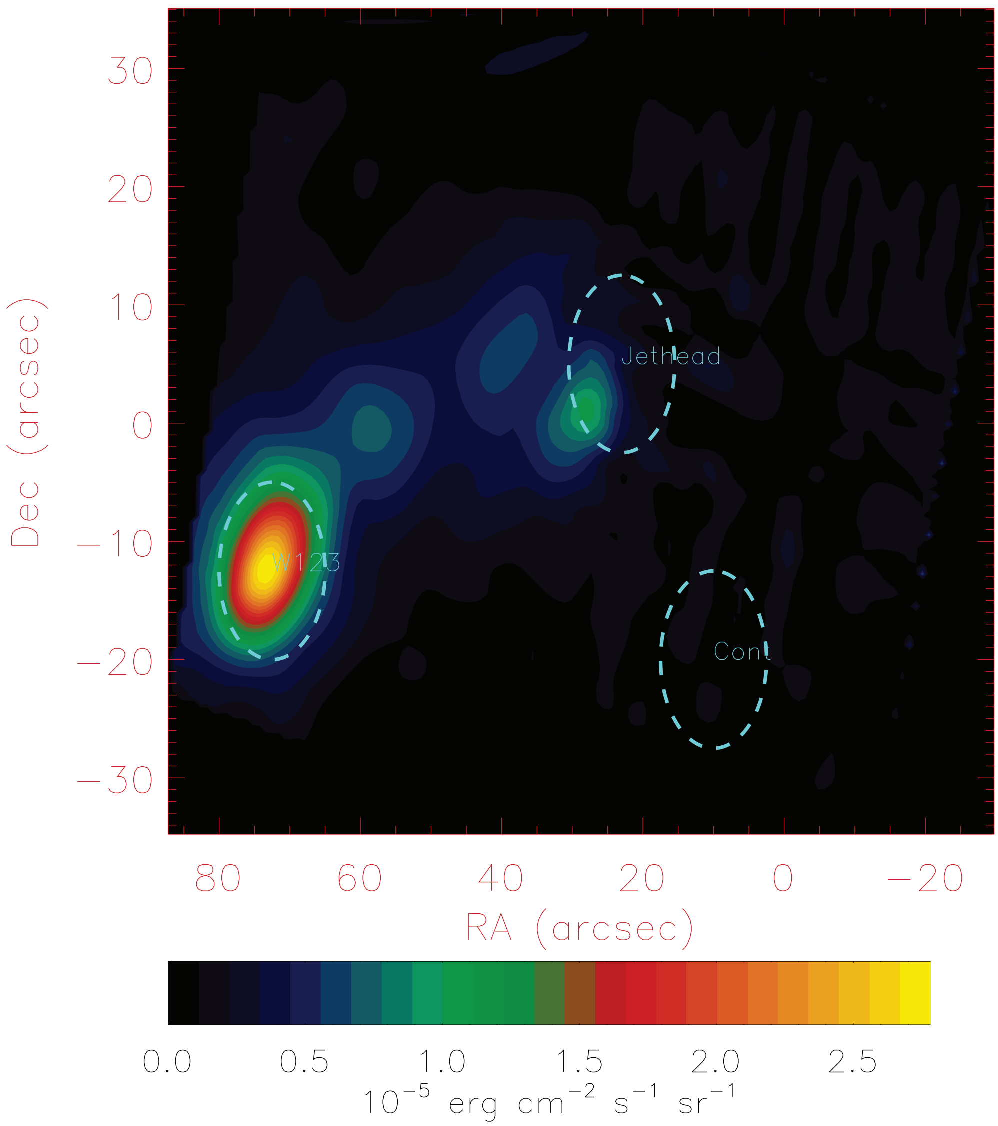

Fig. 1.— Location of the 15” HPBW apertures used to extract individual spectra in GGD 37, overplotted on the [O IV] line map.

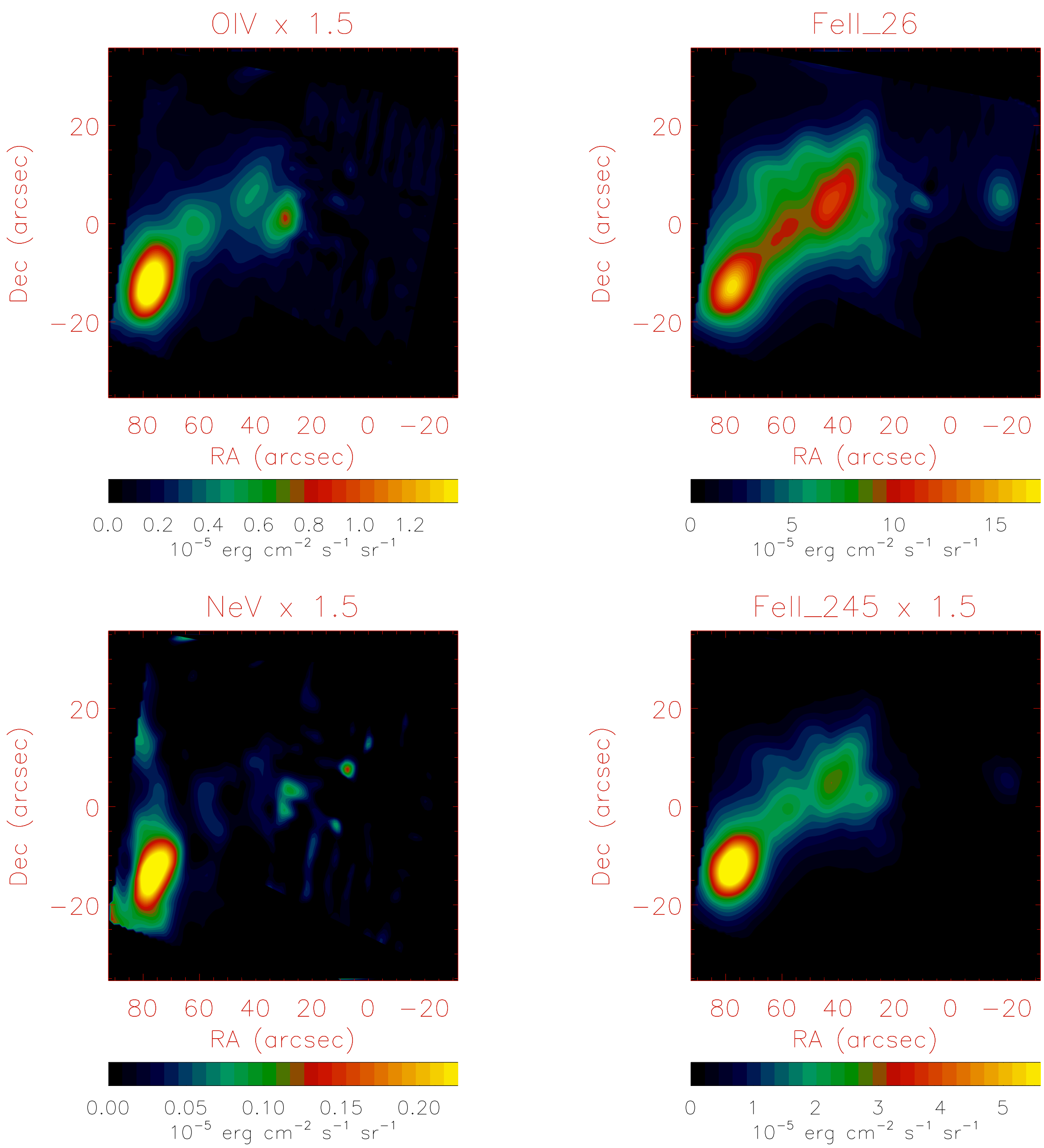

Fig. 2.— Top Left: Map of [O IV] emission from W2 (lower left corner) to the edge of the ionized flow (upper right corner). The emission peaks at two additional locations in the map: first, at the convergence of W1/W2/W3, and second at a point just inside the edge of the flow of lower ionization spectral lines. Top Right: The same region of sky mapped in [Fe II] 26 μm for comparison. Bottom Left: The same plot for [Ne V] emission. Bottom Right: [Fe II] 24.5 μm. Although the [Ne V] detection is weak, the spatial distribution of the emission suggests that it is real, and spatially distinct from the stronger [Fe II] emission.

Table 1. Surface Brightness by Chemical Species by Aperture

Species	Wavelength (μm)	Module	W123 Intensity	Jethead Intensity
[O IV]	25.9	LH	4.00	2.46
[Ne V]	24.3	LH	0.48	0.23
[Ne III]	15.5	SH	78.9	29.6
[Ar III]	21.8	LH	0.36	–

Note. — Surface brightness in units of 10^{-6} erg/cm^2/s/sr of all species at 15" HPBW apertures of three regions of interest: the W1-W2-W3 emission complex (W123), the extreme NW end of the GGD 37 flow (Jethead), and a selected region devoid of structure in the southeastern corner of the map (Continuum Region); see Figure 1. In order to integrate the different modules, we utilized the flux of the [Ne II] and the continuum level as a normalization constant; the SH fluxes are thus decreased by a factor of $\sim$ 4.5 from observed values, and the SL2 spectra are decreased by 1.33 to match continuum levels with SL1. A " – " marking indicates a non-detection or failed linefit.

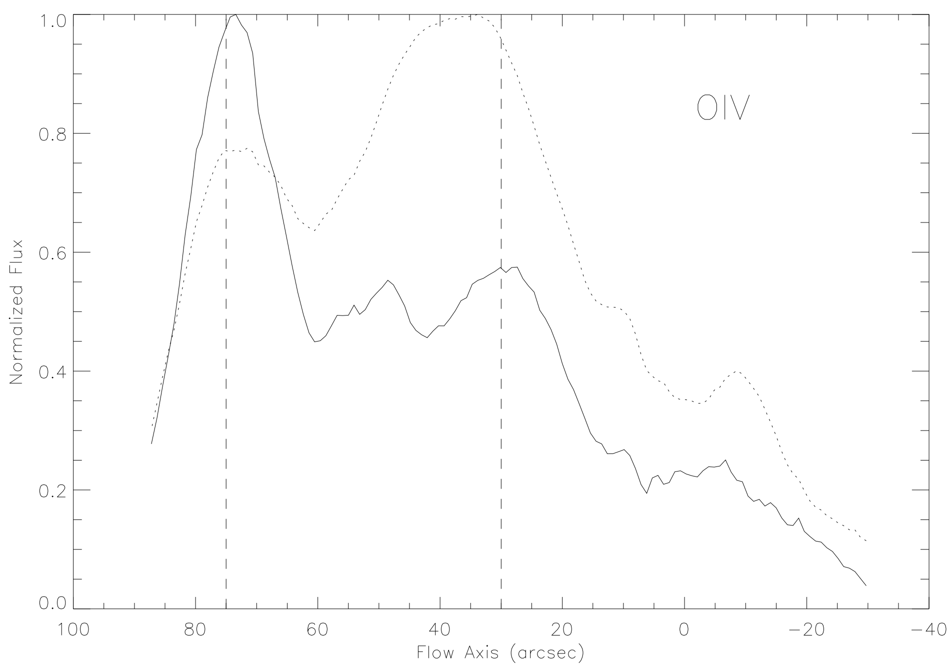

Fig. 3.— Comparison of the peak of bow shock emission in a high excitation line, [O IV], and a lower excitation line, [Fe III], in terms of normalized flux (vertical axis), as a function of position on the flow axis (rotated 40 degrees), similar to the analysis in Raines (2000). The solid curve represents [Fe II]. The dashed line represents [O IV]. The vertical line represents the westernmost peak of [O IV], for comparison.

eV in the case of [Ne V]. The ratio of [Ne II]/[Fe II] (26 μm) which peaks in the vicinity of W2, is 10-20 – much larger than is seen in other intermediate-mass YSO (e.g. HH 54 or HH 7-11 Neufeld et al. 2006b). The [Ne III]/[Ne II] ratio is $\sim$ 0.2-0.5 in this region, gradually falling off to the west before peaking slightly again at the edge of the flow, although it should be noted that this may be confused by separate excitation mechanisms. Ne+ ions can be produced in T Tau disks by X-ray absorption in the warm disk, and the recombination of Ne ions is slow. Ne++ has only weak charge transfer, and Ne+ none at all, with H (Glassgold et al. 2007). This is of importance in analyzing [Ne II] in protoplanetary disks. In the present case the [Ne III] and [Ne II] emission regions are so similar in shape, they are likely to be excited the same way, in an extended and unusually powerful protostellar outflow. The spectra closely resemble that of a supernova remnant, although there are several differences – the lack of certain lines such as [P II] 32.5 μm and [Ne III] at 36 μm (Neufeld et al. 2007), although the latter is probably too faint to be detected in this case. Additionally, [O IV] and [Ne V] are not observed in HII regions.

Published models (e.g. Hollenbach & McKee 1989, hereafter HM89) don't seem to account for the observed line ratios, however. The first problem comes in measuring the mechanical luminosity of the flow from cooling rates. [O I] 63 μm is modeled as the principal cooling line, and [Fe II] and [Si II] are both expected to trace [O I]. Predicted intensity ratios of [Fe II]/[O I] and [Si II]/[O I] are $\sim$ 0.1 for most values of n_e and shock speed, as these lines are also optically thin. [O I] intensity is proportional to the total mass flow through the shock boundary; using the "W123" aperture we calculated an expected intensity of $\sim 2 \times 10^{-4}$ erg s^{-1}cm^{-2}sr^{-1}, and the resulting mass flow rate is 10^9 n_0 v_s. Assuming a fast shock velocity of 100 km/s, and a density of 2×10^4 cm^{-3}, the mass flow rate is 3.3×10^{-6} $M_\odot$ yr^{-1}. If instead we perform the same calculation with [Si II] (34.8 μm), the mass flow is 5.4×10^{-5} $M_\odot$ yr^{-1}, nearly 10 times higher. This is due to the ratio of [Si II]/[Fe II] flux > 1 over the entire flow, which does not match any conditions in HM89. Although the [Si II] and [Fe II] emission are morphologically quite similar, this may reflect differing critical densities, or a high Si/Fe abundance compared to solar values. However this is more likely because HM89 do not include sufficiently fast outflows.

The second problem is the lack of predictions from HM89 for fluxes of high-excitation species such as [Ne V] and [O IV]. The Mappings III Shock Model Library (Allen et al. 2008) predicts mid-IR flux ratios, as already noted for the case of [Ar III]. The [Ne II]/[O IV] ratio is $\sim$ 500 in the W2 region and 190 at the leading edge of the flow. The ratio of [Fe II] (26 μm) to [O IV] is 14.3 and 41.8, respectively. [Ne III]/[Ne II] is $\sim$ 0.21 and 0.15, respectively. [S IV] is not detected, but an upper bound to [S IV]/[S III] is $\sim$ 0.11 and 0.35. The relative lack of [O IV] compared to [Ne II] and [Fe II] predicts a large shock velocity of 500 km/s or more, without a precursor. The lack of [S IV] and relatively high [Ne III] flux seem to indicate a slower 200 km s^{-1} shock, but still without a precursor. Mappings III is far too low in density (and therefore in recombination rates), and does not fit the observed line ratios either.

The final problem comes in modeling simultaneously the molecular emission and the high-excitation lines. Flower et al. (2003) model GGD 37 itself with a 25 km s^{-1} J-shock with a magnetic precursor, which matches the H_2 emission well but is not nearly fast enough to produce the high-excitation lines. However, in advance of detailed complex modeling we can make some cruder estimates of shock energetics that are implied by these lines and the X-ray emission.

We can estimate the shock speed from detailed balance from excitation by UV/X-ray emission, as a function of the ratio of [Ne V]/[O IV]. The highest temperature achieved in the shock is given by the [Ne V] 97 eV transition, indicating a temperature of 4×10^6 K. We can calculate the shock speed from the observed temperature and luminosity (e.g. Watson et al. 2007). Assuming a solar abundance ratio of O/Ne ~ 8, we derive a post-shock temperature of 18,100 K for the observed [O IV]/[Ne V] ratio of ~ 10. This indicates a post-shock velocity of only 24 km/s. Furthermore, Schneider et al. (2009) posit that the entire flow is one continuous flow of shock-heated material with a velocity in the hundreds of km s^{-1}. The approximate emitting volume is $\sim 4 \times 10^{52}$ cm^3, and the derived n_e of emitting plasma is ~ 10 cm^{-3} in that region. Thus we find a total shocked mass 0.62 $M_\odot$ for a density of 2×10^4 cm^{-3}. The total momentum of the flow is then 124 $M_\odot$ km s^{-1}, assuming a fast shock speed of at least 200 km s^{-1}. This is quite high compared to other powerful flows observed with Spitzer-IRS (e.g. 1-2 $M_\odot$ km s^{-1} for HH 7-11; Maret et al. 2009), further evidence that GGD 37 is unusual.

If we propose a single emitting region containing all three observed ionization states of Ne (Ne+, Ne++, Ne++++), supposing the hot postshock gas is uniform in n_e and T, and the ionization states are in equilibrium, we could in theory estimate the physical conditions. However under these assumptions it is impossible for a single region to produce all three lines simultaneously. Thus comparable intensities of all three transitions suggests either a photoionizing source or a collisionally ionizing source – in either case, likely a powerful and extremely hot jet, highlighted by the X-ray emission region (Figure 4).

A detailed discussion of the H_2 emission, as well as the [Fe II] and other fine structure line maps will be explored in subsequent papers.

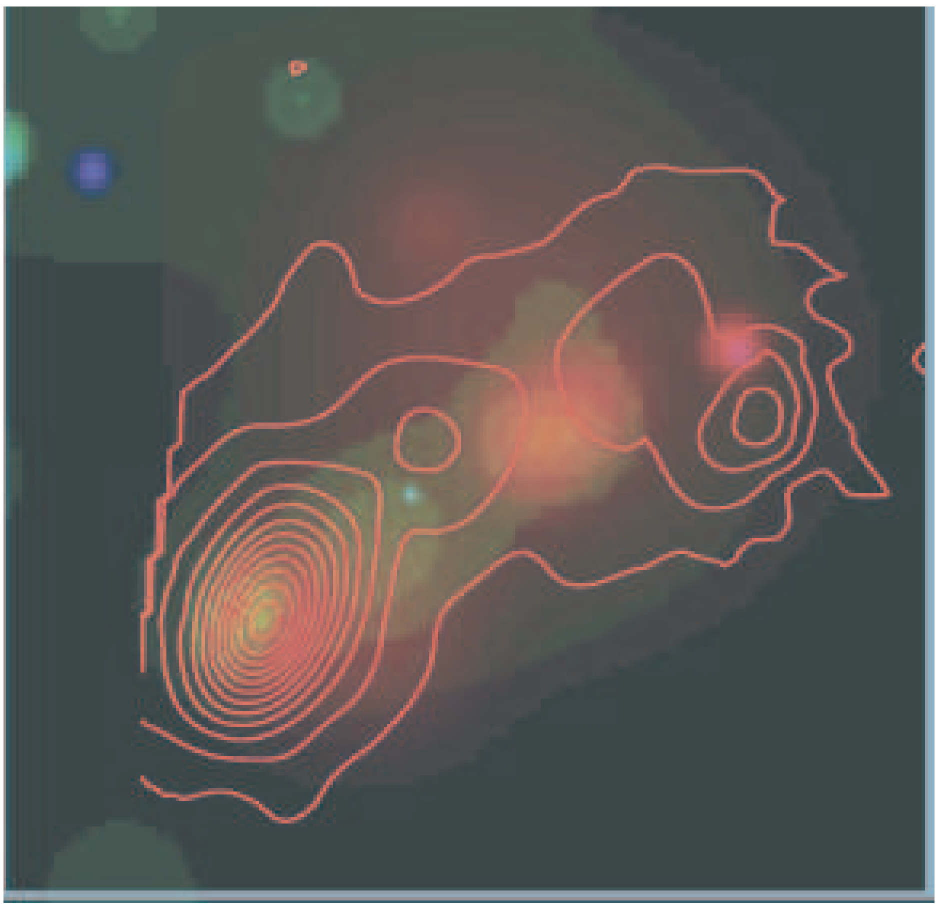

Fig. 4.— Color contour map of 0.3-1.5 keV X-ray emission of a 1' × 0.8' region in GGD37; overplotted in red unfilled contours is the [O IV] Spitzer-IRS emission, overlaid in color intensity contours is the [O IV] emission from W2 (lower left corner) to the edge of the ionized flow (upper right corner). The correlation between [O IV] and X-ray emission is apparent.

4. Conclusions

We present the detection of [Ar III], [O IV], and [Ne V] fine structure lines, the highest appearance potential for optical or infrared lines ever detected in the vicinity of a Herbig-Haro flow. Considering this data along with 0.2-1.0 keV X-ray maps of the flow, we suggest that GGD 37 is the hottest HH object detected so far.

The apparent extended nature of the high ionization energy lines and soft X-ray emission from the HH 168 flow suggests that it is extraordinarily hot for a Herbig-Haro object, perhaps an indirect detection of a radiative jet. In agreement with models of planar C+J shocks, we detect a significantly extended transitional boundary layer. This suggests that the radio source W2 is a plausible candidate for an edge-on high mass embedded protostar driving an outflow to the northwest.

The authors would like to thank Neal Evans, Mike Dunham, Manoj Puravankara, Dave Pooley, and Peter Yoachim for helpful comments and discussion. This work is based on observations made with the *Spitzer Space Telescope*, which is operated by the Jet Propulsion Laboratory, under NASA contract 1407. Support for this work was provided by NASA through contract 1257184. This research was supported in part by Jet Propulsion Laboratory (JPL) contract 960803 to Cornell University, and Cornell subcontracts 31419-5714 to the University of Rochester. This research has also made use of the SIMBAD database, operated at CDS, Strasbourg, France.

REFERENCES

Allen, M. G., Groves, B. A., Dopita, M. A., Sutherland, R. S., & Kewley, L. J. 2008, ApJS, 178, 20

Bally, J., Feigelson, E., & Reipurth, B. 2003, ApJ, 584, 843

Draine, B. T. 1980, ApJ, 241, 1021

Favata, F., Fridlund, C. V. M., Micela, G., Sciortino, S., & Kaas, A. A. 2002, A&A, 386, 204

Flower, D. R., Le Bourlot, J., Pineau des Forêts, G., & Cabrit, S. 2003, MNRAS, 341, 70

Froebrich, D., Smith, M. D., & Eislöffel, J. 2002, A&A, 385, 239

Garay, G., Ramirez, S., Rodriguez, L. F., Curiel, S., & Torrelles, J. M. 1996, ApJ, 459, 193

Glassgold, A. E., Najita, J. R., & Igea, J. 2007, ApJ, 656, 515

Guiles, S., Bernard-Salas, J., Pottasch, S. R., & Roellig, T. L. 2007, ApJ, 660, 1282

Hartigan, P., & Lada, C. J. 1985, ApJS, 59, 383

Hartigan, P., Lada, C. J., Tapia, S., & Stocke, J. 1986, AJ, 92, 1155

Hollenbach, D., & McKee, C. F. 1989, ApJ, 342, 306

Hughes, V. A. 1989, AJ, 97, 1114

Hughes, V. A., & Wouterloot, J. G. A. 1982, A&A, 106, 171

Maret, S., Bergin, E. A., Neufeld, D. A., Green, J. D., Watson, D. M., Harwit, M. O., Kristensen, L. E., Melnick, G. J., Sonnentrucker, P., Tolls, V., Werner, M. W., Willacy, K., & Yuan, Y. 2009, ApJ, 698, 1244

Neufeld, D. A., Green, J. D., Hollenbach, D. J., Sonnentrucker, P., Melnick, G. J., Bergin, E. A., Snell, R. L., Forrest, W. J., Watson, D. M., & Kaufman, M. J. 2006a, ApJ, 647, L33

Neufeld, D. A., Hollenbach, D. J., Kaufman, M. J., Snell, R. L., Melnick, G. J., Bergin, E. A., & Sonnentrucker, P. 2007, ApJ, 664, 890

Neufeld, D. A., Melnick, G. J., Sonnentrucker, P., Bergin, E. A., Green, J. D., Kim, K. H., Watson, D. M., Forrest, W. J., & Pipher, J. L. 2006b, ApJ, 649, 816

Pravdo, S. H., & Tsuboi, Y. 2005, ApJ, 626, 272

Pravdo, S. H., Tsuboi, Y., Uzawa, A., & Ezoe, Y. 2009, ApJ, 704, 1495

Raines, S. N. 2000, PhD thesis, AA(THE UNIVERSITY OF ROCHESTER)

Reipurth, B., & Raga, A. C. 1999, in NATO ASIC Proc. 540: The Origin of Stars and Planetary Systems, ed. C. J. Lada & N. D. Kylafis, 267–+

Schneider, P. C., Guenther, H. M., & Schmitt, J. H. M. M. 2009, ArXiv e-prints

Sonnentrucker, P., González-Alfonso, E., Neufeld, D. A., Bergin, E. A., Melnick, G. J., Forrest, W. J., Pipher, J. L., & Watson, D. M. 2006, ApJ, 650, L71

Watson, D. M., Bohac, C. J., Hull, C., Forrest, W. J., Furlan, E., Najita, J., Calvet, N., D'Alessio, P., Hartmann, L., Sargent, B., Green, J. D., Kim, K. H., & Houck, J. R. 2007, Nature, 448, 1026

Wright, C. M., Drapatz, S., Timmermann, R., van der Werf, P. P., Katterloher, R., & de Graauw, T. 1996, A&A, 315, L301